EFFECTS OF SEVERE PLASTIC DEFORMATION INDUCED BY EQUAL-CHANNEL ANGULAR PRESSING IN THE AA1200, AA5754, AA6082 AND AA6106 MODIFIED WITH ZR AND ZR+SC

M. Cabibbo, C. Scalabroni, E. Evangelista
Dip. Meccanica, Università Politecnica delle Marche - Ancona, Italy

Abstract

The microstructure evolution under elevated plastic deformations was investigated by means of transmission electron microscopy (TEM) in different aluminium alloys processed by the equal channel angular pressing (ECAP) technique in route Bc to strain of 8. The alloys was characterized by submicron-scale grains. The AA1200 high-angle boundaries (misorientation higher than 15°) accounted for ~70% of all boundaries. In the AA5754 measurements indicated average grain sizes of about 0.3–0.4 μm in the as-pressed condition, thereby demonstrating that ECAP is an especially effective procedure for attaining an ultrafine grain size. It appeared that many of the grain boundaries were ill-defined and it is reasonable to assume that, as in an earlier report on ECAP of commercial Al alloys, these boundaries are in high-energy non-equilibrium configurations. For the AA6082 different kinds of alloys have been investigated, the first alloy (commercial AA6082) has a microstructure evolution depending on the presence of Mg_2Si and Si particles, the others alloys (with Zr and Sc+Zr) have a microstructure stabilized by the dispersoids.

Riassunto

L'evoluzione microstrutturale di alcune leghe che hanno subito severe deformazioni plastiche ad opera del processo ECAP è stata investigata attraverso indagini al microscopio a scansione elettronica (TEM). La deformazione impartita è arrivata ad un livello pari ad μ=8 seguendo la route B_C. Le leghe sono caratterizzate da una dimensione dei grani di scala sub-micrometrica. Nella lega AA1200 i bordi ad alto angolo arrivano al 70% dei bordi visualizzati, nella AA5754 la dimensione media dei grani dopo la deformazione arriva a 0.3-0.4 μm, questo e altri risultati che vedremo in seguito dimostrano come l'ECAP sia un processo effettivamente efficace per l'affinamento microstrutturale con la possibilità di ottenere materiali con attitudini superplastiche.

Molti dei bordi di grano sembrano mal definiti ed è ragionevole supporre che, come riscontrabile nella bibliografia riguardante l'ECAP di leghe commerciali di Al, questi bordi sono in configurazioni ad alta energia di non-equilibrium. Per la lega AA6082 oltre a quella commerciale sono state studiate, delle leghe modificate con l'aggiunta di alliganti particolari. La prima lega (AA6082 commerciale) ha uno sviluppo della microstruttura determinato dalla presenza delle particelle del silicio e di Mg_2Si, nelle altre in cui vediamo aggiounti alla lega Zr e Sc+Zr la microstruttura è determinata e stabilizzata dalla presenza di dispersoidi.

INTRODUCTION

Different techniques for producing ultrafine-grained (UFG) materials for structural applications have been introduced and patented, especially in the last decade [1]. The advantages of fabricating materials with sub-micron size grained microstructure as structural components lie in their improved mechanical properties such as strength, hardness, ductility, fatigue resistance and low-temperature superplasticity [1-10]. Equal channel angular pressing (ECAP), introduced and developed by Segal *et al.* and Segal [1,3], is a promising technique that uses severe plastic deformation (SPD) to refine microstructure. ECAP has the important advantage to maintain billet shape. A typical ECAP die, Fig. 1, consists of two intersecting channels of identical cross-section. A billet of material is introduced in the vertical channel and forced by a plunger into the horizontal one. Shear strain per pass through the die is determined by the angles of channel intersection and curvature [6,11,12]. Many processing parameters have dramatic effects on the resulted microstructure [12]: die angles (determining the strain introduced into the material), the number of passes (accumulation of strain), deformation route (critical parameter for texture and microstructure evolution with strain), and also the extrusion speed, temperature, friction. Langdon and co-workers [6,10] found the angles $\Phi = 90°$ and $\Psi = 20°$, Fig. 1 and eq. 1, to be the most efficient, while the extrusion speed and specimen-die channel friction have minor influence on the refining process. A number of theories have been proposed to explain the effect of processing routes on the microstructure. Iwahashi *et al.* [11] and Furukawa *et al.* [12,13] proposed that route Bc (90° rotation of the billet at each pass) is most favorable for producing a microstructure consisting of essentially uniform and equiaxed grains separated by high-angle boundaries (HABs). This was suggested to be due to crossing shear planes, and to a regular restoration into equiaxed structure during consecutive pressing. Sun et al. [14,15] studied the different routes: (A, B_A, B_C, and C, where the route A refers to repetitively pressing the sample without any rotation, the route B_A refers to a rotation of 90¡ back and forth between each pass, route B_C refers to a rotation of 90° between each pass and route C refers to a rotation by 180° between each pass as a function of different microstructure parameters. They found that the effectiveness in terms of formation of HABs was A>Bc>C, in terms of reducing grain size was Bc>A>C and in terms of generating equiaxed grains was Bc>C>A. Studies on cell and grain evolution have been performed only in recent years [4,16-21,23,24]. Several investigations [12-15,22-32] have shown that, during deformation [23,24], grains subdivide into many small crystallites, each having a crystal rotated orientation. Thus, during straining, dislocations generally arrange into a mosaic-like pattern. The mosaic-like configuration is basically composed of boundaries surrounding regions with relatively low dislocation density. Studies on metals established that grains were fragmented into domains of different slip systems, called cell blocks, during deformation [24,27].

Concerning the Zr and Sc+Zr dispersoids, several studies have shown that aluminium alloys, alloyed with scandium, or zirconium, have excellent mechanical properties at room temperature, due to the presence of coherent, nanometre size $Al_3Sc(Zr)$ precipitates effectively dispersed either

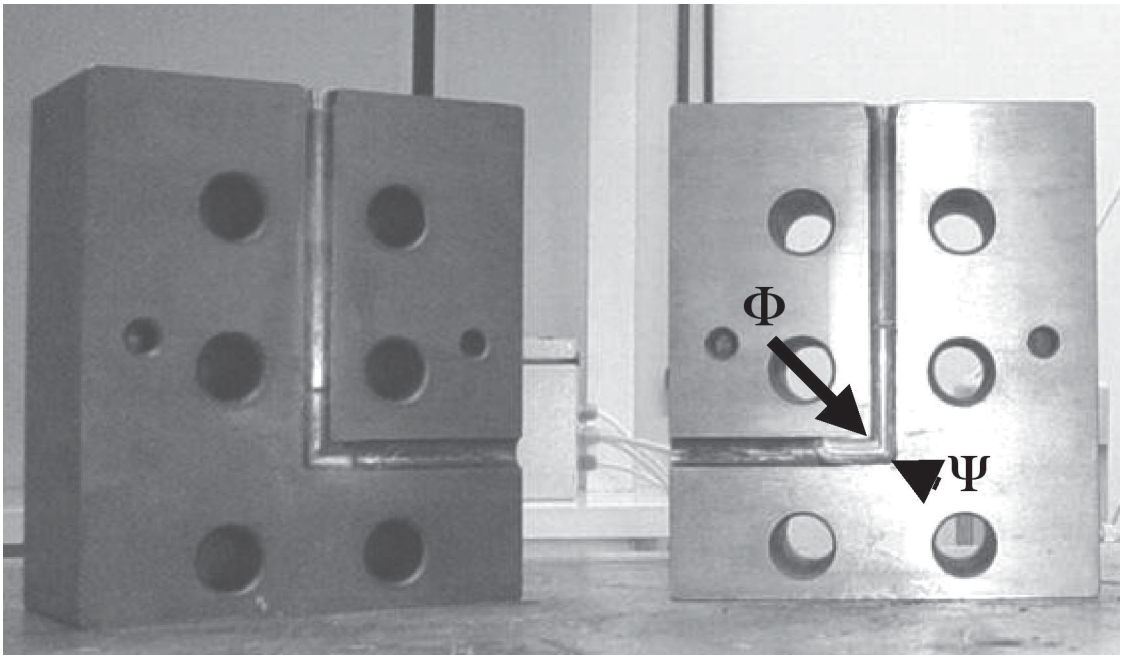

Fig. 1: Open solid ECAP die used in this study. The intersection and curvature angle values are $\Phi = 90°$ and $\Psi = 20°$ respectively (see eq. 1).

in the grain boundaries and within grains, thus blocking mobile dislocations and stabilizing a fine-grained structure [33,34]. These $Al_3Sc(Zr)$ precipitates are stable up to the typica recrystallisation temperatures for aluminium alloys [35]. Combined additions of Sc and Zr were shown to be more effective in refining as-cast material microstructures; in particular, Zr is able to replace some of the Sc in Al_3Sc, giving rise to $Al_3(Sc_{1-x},Zr_x)$ dispersoids having an L12 crystal structure like the Al_3Sc [33-35].

The present paper describe results on the deformation mechanisms induced by ECAP in some extensively used aluminum series alloys: AA1200, AA5754, AA6082 and AA6106 modified with Zr and Zr+Sc (hereafter: Alloy 1 and Alloy 2).

EXPERIMENTAL DETAILS

The chemical composition of the tested alloys is reported in Table 1. The alloys were cast into a rod-shaped bars 10 mm in diameter.
Before ECAP processing, the AA 6000 alloys were full annealed and a T8 treatment was carried out in the Alloy 1 and Alloy 2. The die was placed in a dedicated pressing machine with a maximum load of 80-100 kN and a pressing speed of 4 mm min^{-1}, operating at room temperature. The die was constituted of two blocks of SK3 tool steel (Fe-1.1%C), which were bolted together to give a single internal L-channel 10 mm in diameter (Fig. 1). The two cylindrical channels, intersected at an angle $\Phi = 90°$ and a curvature $\Psi = 20°$. Samples and channels were coated with a spray lubricant containing MoS_2.
Based on Eq. 1, this configuration allowed to introduce a true strain of $\varepsilon = 1.055$ at each pass (N) [3,18,37].

$$\varepsilon_N = \frac{N}{\sqrt{3}}\left[2\cot\left(\frac{\Phi}{2}+\frac{\Psi}{2}\right)+\Psi\,\mathrm{cosec}\left(\frac{\Phi}{2}+\frac{\Psi}{2}\right)\right]$$

Table 1 - Chemical composition (wt%).

Alloy	Mg	Mn	Cr	Ti	Cu	Si	Fe	Zn	Zr	Sc	Cu+Mn
AA1200	---	---	---	---	---	0.7	0.3	0.1	---	---	0.05
AA5754	2.5	0.3	0.4	---	0.1	0.4	0.4	0.2	---	---	---
AA6082	1.193	0.650	0.010	0.015	0.005	1.019	0.267	---	---	---	---
Alloy 1	0.34	0.014	---	---	---	0.51	0.16	---	0.10	---	---
Alloy 2	0.34	0.014	---	---	---	0.51	0.16	---	0.10	0.117	---

Three orthogonal planes (X,Y) were used to define the orientations of the billet deformed by ECAP, where X is perpendicular to the pressing direction, Y is the flow plane, i.e., the one containing the pressing and the transverse direction [10-13,19].
TEM samples were sectioned along the Y plane. Thin foils were prepared by mechanical grinding 1-mm thick slices down to a thickness of 70-90 μm, followed by chemical polishing (1/3 HNO_3 in methanol) in order to minimize the grinding damage. Disks 3 mm in diameter were subsequently thinned with a double-jet electro-polisher using a solution of 20% $HClO_4$ and 80% methyl alcohol at -15°C and 24 V and examined in a Philips CM200 TEM operating at 200 kV, equipped with a double-tilt stage.
Microstructure examination was focused on the cell, grain size distribution and boundary misorientation. Concerning the boundary misorientation, three independent Kikuchi patterns were taken into account, typically either incidental dislocation boundaries (IDBs) and geometrically necessary boundaries (GNBs). As the strain increases the fraction of boundaries that are low-angle boundaries (LABs) decreases steadily. The misorientation angle is defined as minimum rotation angle that can cause the two crystals to coincide each other by selecting an arbitrary rotation axis. Moiré fringes were evaluated, instead of Kikuchi analysis. The misorientation measurement was carried out by counting the number of dark-bright pairs directly on TEM plates and, subsequently, using Eq. (2a) [36,38].

$$D = \frac{d_1 d_2}{\left(d_1^2 + d_2^2 - 2d_1 d_2 \cos\varphi\right)^{\frac{1}{2}}} \qquad (2a)$$

where d_1 and d_2 are the two superimposed crystal lattice spacing, j is the rotational angle and D is the overall width of the resulting Moiré fringes. In the case of simple matrix rotation, Moiré fringes are characterized by an angle j, and $d_1 = d_2$, thus Eq. (2a) reduces, for small angles, to Eq. (2b):

$$D \cong d / \varphi \qquad (2b)$$

RESULTS AND DISCUSSION

Fig. 2 (a) to (d) shows some representative micrographs of the AA1200 illustrating the boundary spacing evolution with strain of either LABs and HABs. Boundary misorientation angles are also reported. Fig. 3 shows the comparison of HAB fraction among the three different routes to which the 1200 alloy has been subjected: route A, C and Bc; the fraction of HABs after 8 passes are 81, 62, 58 %, respectively.

Initially at low strains very coarse deformation bands are formed. As the strain increases block walls develop within the coarse bands. The majority of cells, formed after the first and second passes, were nearly free of dislocations in the interior. After one ECAP pass, cells within the bands are elongated as well as the shearing bands along the shear direction. Mean linear intercept measurements showed that the block walls are 2.68, 1.26, 1.75 mm, in length, and 880, 640, 815 nm, wide, for the sample A-2, C-2 and Bc-2, respectively. In sample A-2 and Bc-2, the dominant features are the parallel bands of elongated block walls inclined at an angle of 45–50° with the pressing direction, depending on the specific strain path, equiaxed cells can also be found in some areas, in sample C-2. For sample Bc-2, the

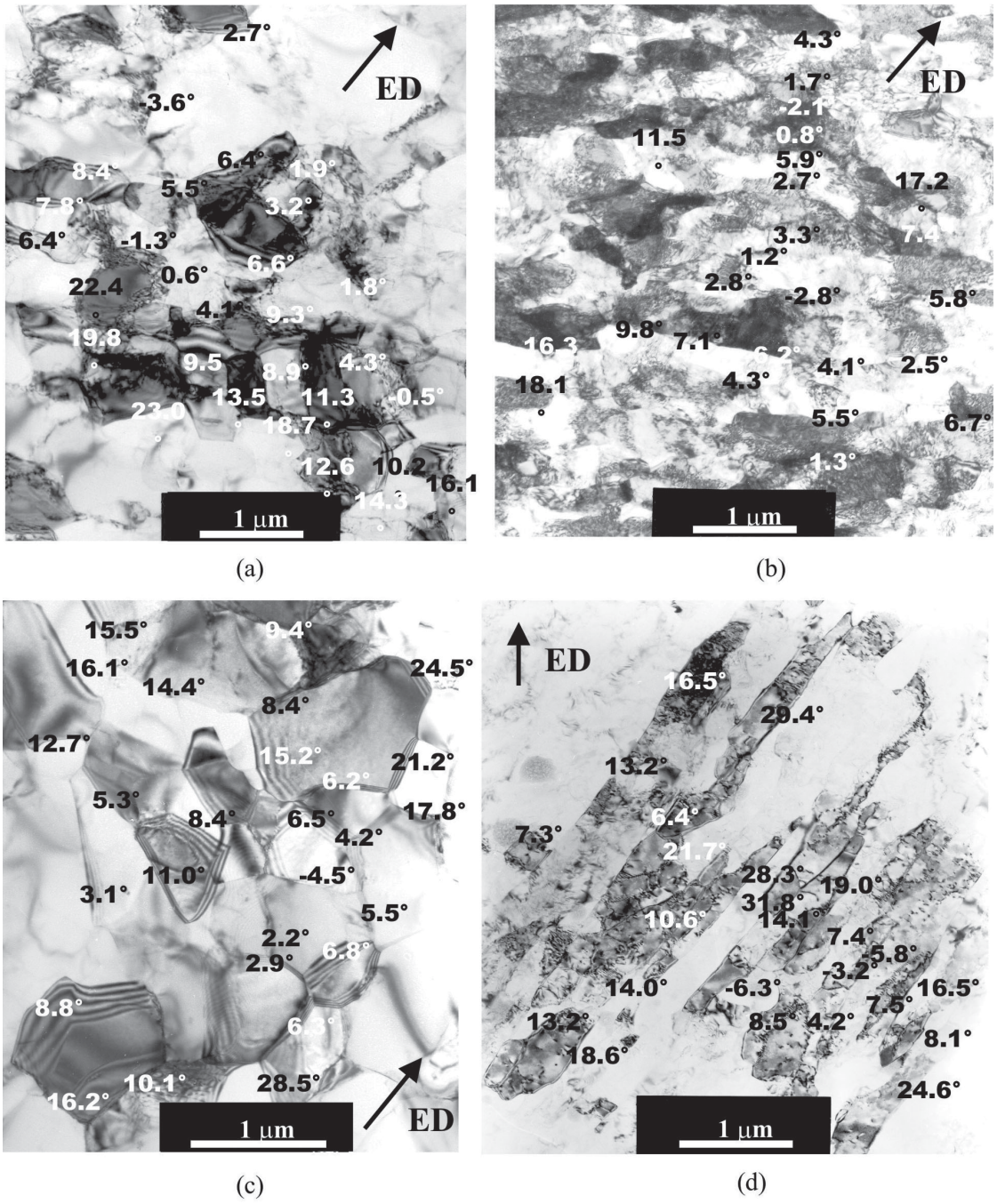

Fig. 2: TEM-BF of the AA1200 showing the deformation process of different straining levels, after 1 (a), 4 (b), 5 (c), 8 passes (d). Some of the boundary misorientation values are also reported. The extrusion direction (ED), i.e. ECA-pressing direction, is indicated.

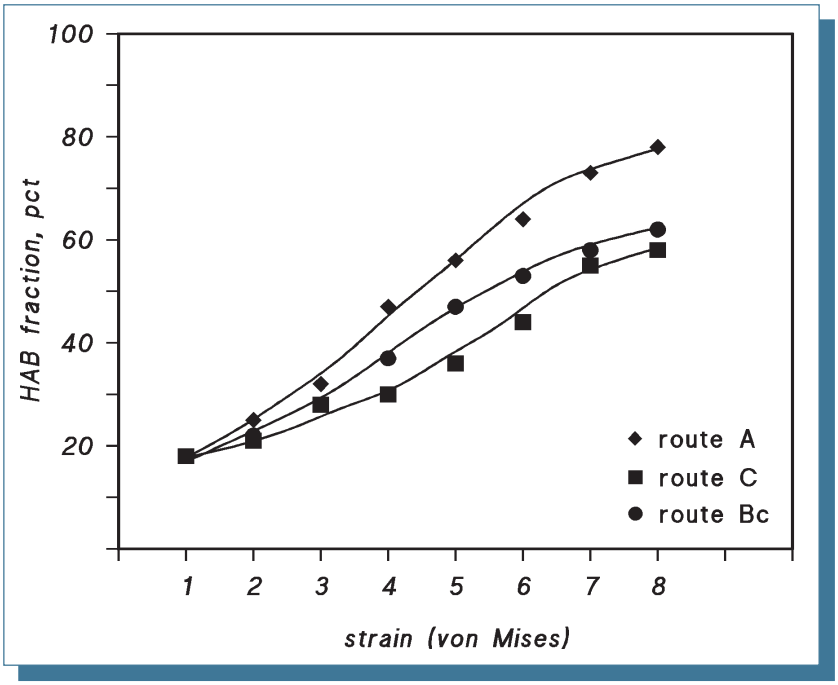

Fig. 3: High angle boundaries (HABs) fraction plots as a function of strain for the three different strain paths.

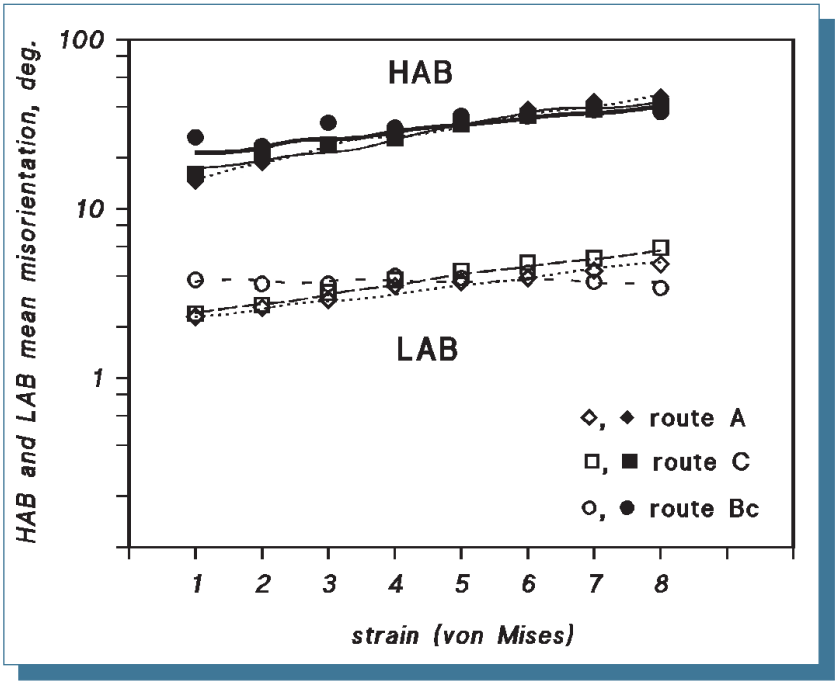

Fig. 4: Misorientation evolution with strain of cells and block walls, for the three strain paths in AA1200.

microstructure consisted of parallel bands of elongated block walls as well as large number of tangled dislocations, although the banded structure is less evident. Fig. 4 is a plot of the LABs and HABs misorientation as a function of strain. The average misorientation angles of LABs and HABs are very close, i.e., 4.2° for LABs and 34° for HABs, among the three strain paths. In terms of the production of HABs, route A is more effective than route Bc, which, in turns, is far more effective than the route C. In route C, the shear plane does not change during repeated pressing and the strain of the first pass can be reversed in the following pass. This route contributes to a redundant strain process and less HABs are generated. Then, the effectiveness in creating HABs is essentially in the sequence: A > Bc > C.

Fig. 5 (a) to (c) shows the misorientation distribution as a function of strain for routes A, C, Bc, respectively. The boundary misorientation distributions have been divided into 15¡ ranges: Low Angle Boundaries (LABs), misorientation less than 15° Low High Angle Boundaries (LHABs), from 15–30°, Medium High Angle Boundaries (MHABs), from 30–45°, and Very High Angle Boundaries (VHABs), with misorientation beyond 45°. Boundary misorientation angles shows nearly constant population evolution toward high mean values, from low to high angles, in the three strain paths. Yet, a bimodal distribution, with a large fraction of low-angle boundary, is found for A and C samples, and an almost constant distribution, from LAB to VHAB, for route Bc (Fig. 5 (a) to (c)). TEM inspections indicate that the billets deformed to large strains by ECAP (8 passes) still have a significant fraction of low-angle boundaries as compared with the boundary misorientation of grains with random Mackenzie distribution. This is attributed to the continuous generation of low-angle boundaries during deformation. This process is more evident in route C and, to some extent, in route Bc, but less pronounced in route A.

On average, the misorientation between adjacent block walls increases with strain and some of them may eventually evolve into new high angle boundaries. LABs retained at very high strains, are typically transverse to the HABs. The HABs often appears as lamellar structures prevalently aligned ~45° to the pressing direction. As the strain increases (up to the maximum strain of e ≅ 8), new HABs progressively evolve at the block walls within the primary deformation bands. These block walls account for the build up of the LHAB fraction, and, at the same time, some of the MHABs may march upwards to VHABs. The strain direction of

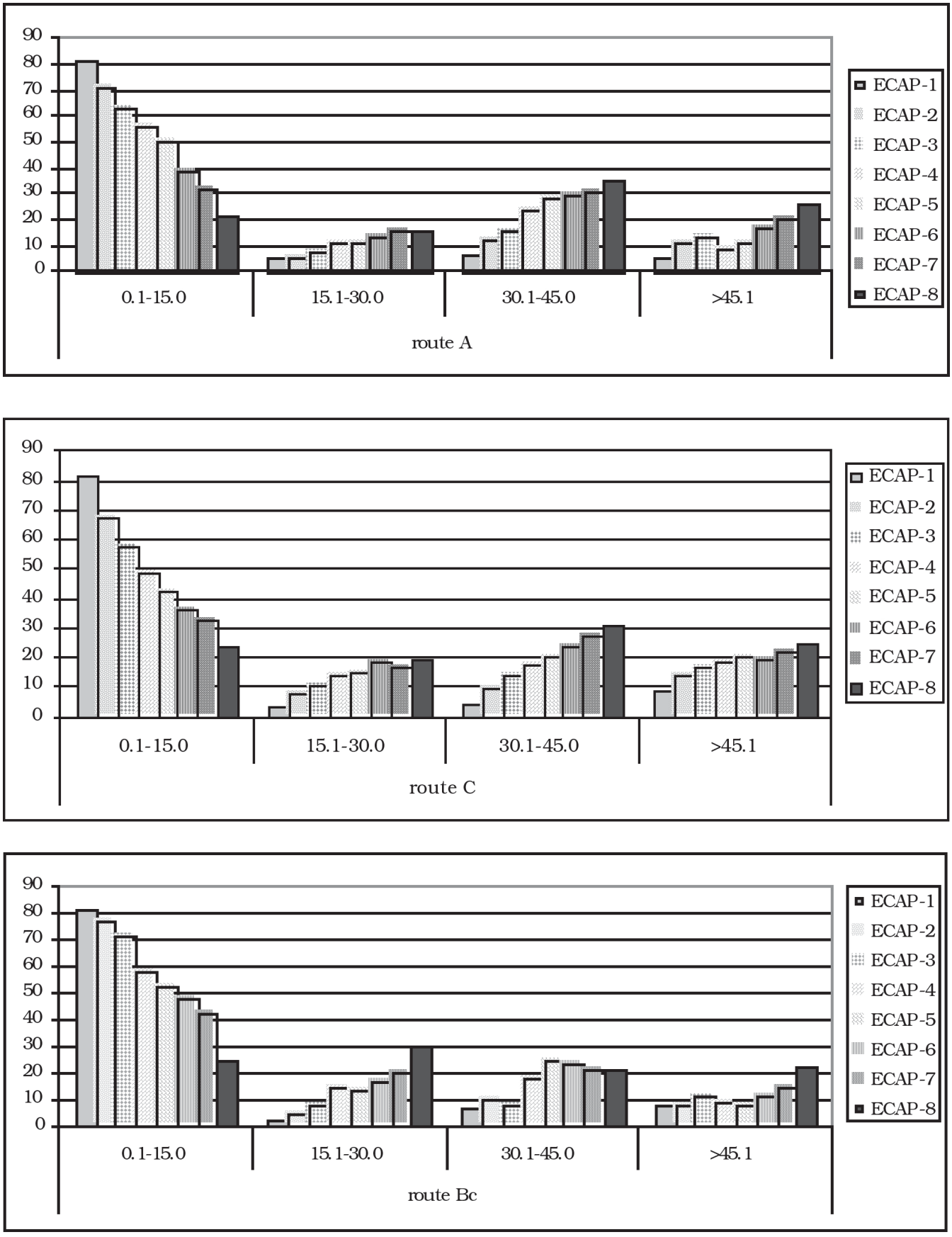

Fig. 5: AA1200: cumulative misorientation distribution of LABs, LHABs, MHABs and VHABs, corresponding to misorientation ranges of (0.1°-15°), (15.1°-30°), (30.1°-45°) and above 45.1°, respectively; route A (a), route C (b), route Bc (c).

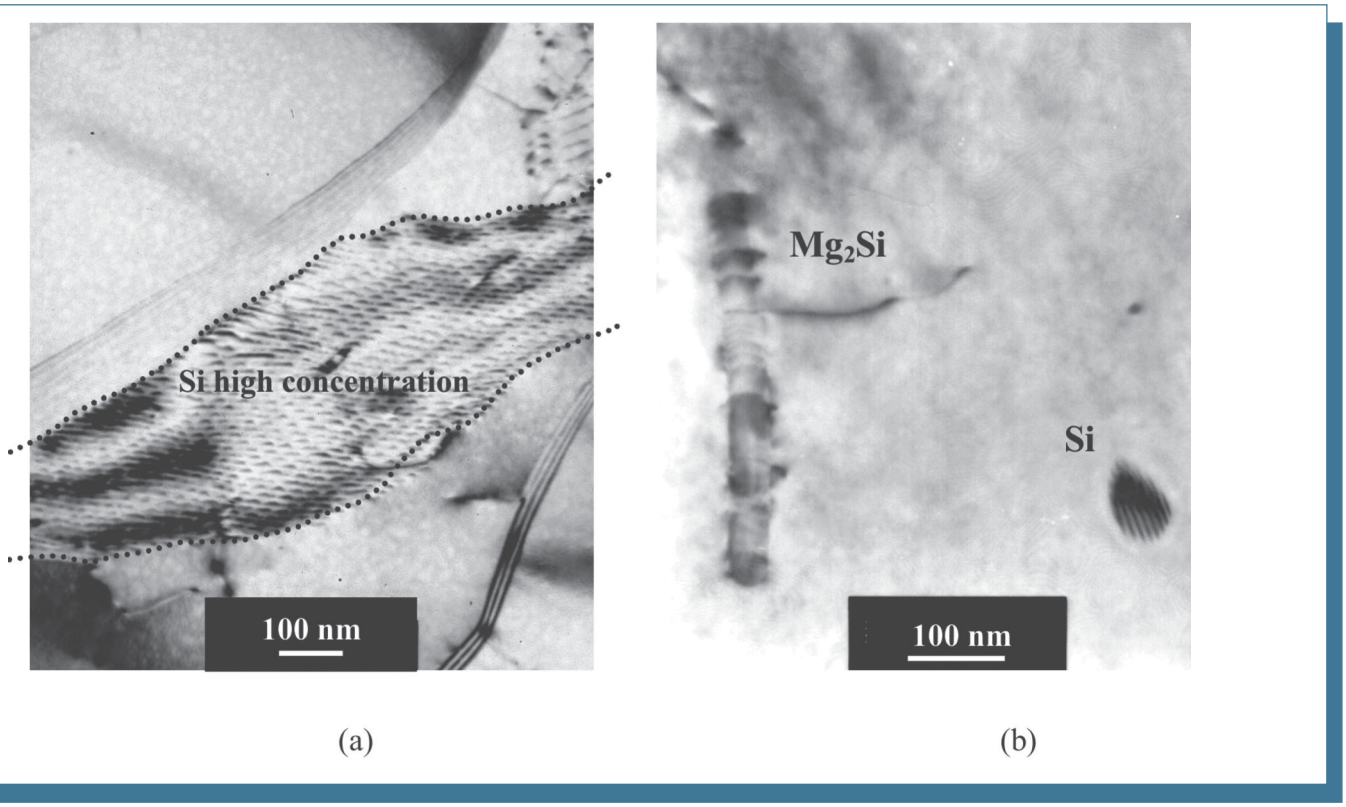

Fig. 6: TEM micrographs of AA6082 after 6 passes; a detail of a grain boundary in which Si particles are dissolving (a), an example of Mg_2Si fragmentation and Si-particle re-absorption processes during ECAP deformation.

route Bc changes every pass therefore contributes intersections, which develop a near spatially uniform network in the material, and consequently leads to a higher efficiency in HAB generation. Microstructural examinations of billets pressed through 2 to 6 passes, of the alloy AA5754 revealed an array of reasonably equiaxed grains having average sizes of <1 μm (see also [39]). Selected area electron diffraction patterns after 6 passes showed diffuse rings and evidence for the presence of an array of grains with high disoriented angles. Measurements indicated average grain sizes of about 0.3–0.4 μm in the as-pressed samples. It appeared that many of the grain boundaries were ill-defined and it is reasonable to assume that, as in an earlier report on ECAP of AA1200 [38], these boundaries are in high-energy, non-equilibrium configurations. The effect of severe plastic deformation on the secondary phase particles (Si and Mg_2Si) studied by means of TEM inspections, showed a much higher volume fraction of very-fine b" metastable particles (with a mean equivalent diameter in the range: 130 - 95 nm after 6 passes) than prior to deformation. Now, these particles have a slightly smaller volume fraction and a greater mean spacing. This means that both fragmentation of the Mg_2Si particles and partial dissolution and redistribution of Mg and Si in the Al-matrix took place (see also [40]). Representative TEM and SEM-EDS analyses of the material after 6 passes, Fig 6 (a),(b), shows a partial dissolution, of Mg and Si previously forming long, needle-like Mg_2Si particles, fragmented by glide dislocations created by the severe plastic deformation. It is interesting to note that the first ECAP pass is responsible for the Mg_2Si fragmentation and for partial dissolution of the Si particles. Thus, the Mg_2Si refinement into finer particles effectively contributed to the hardening by pinning dislocations.

Fig. 7 (a),(b) shows some representative TEM images of Alloy 1 and Alloy 2. In that case a strain of about 12 have been obtained. The cells, which were found to contain high levels of interior dislocations, had a mean size of ~2 °m after the first pass in presence of Sc, and of ~5 °m in the other material; cell boundary misorientation was mainly of 4-5¡, and 1-2¡, respectively. Cell size shrank with strain more effectively in Alloy 2, reaching a mean size of ~330 nm, after 8 passes, and ~250 nm after a strain of 12, while it was considerably less pronounced in Alloy 1, reaching the value of ~720 nm, after 8 passes, and ~450 nm at a strain of 12. The cell boundary misorientation increased much more in the presence of the $Al_3(Sc_{1-x},Zr_x)$ to a mean value of ~8¡, compared with ~5¡ in Alloy 1. In the Alloy 1, the Al_3Zr particles are mostly coherent and heterogeneously distributed throughout the matrix; in Alloy 2, the Sc-containing particles are much more homogeneously distributed. The deformation and microstructure refining mechanism is believed to be greatly influenced by the spatial distribution and size of the fine dispersoids. In a sense, they act as preferential deforming paths for the deformation bands, which control the refining process.

Dispersoids pin not only free dislocations, but, if possible, even more effectively, also cell boundaries and the newly introduced deformation bands,

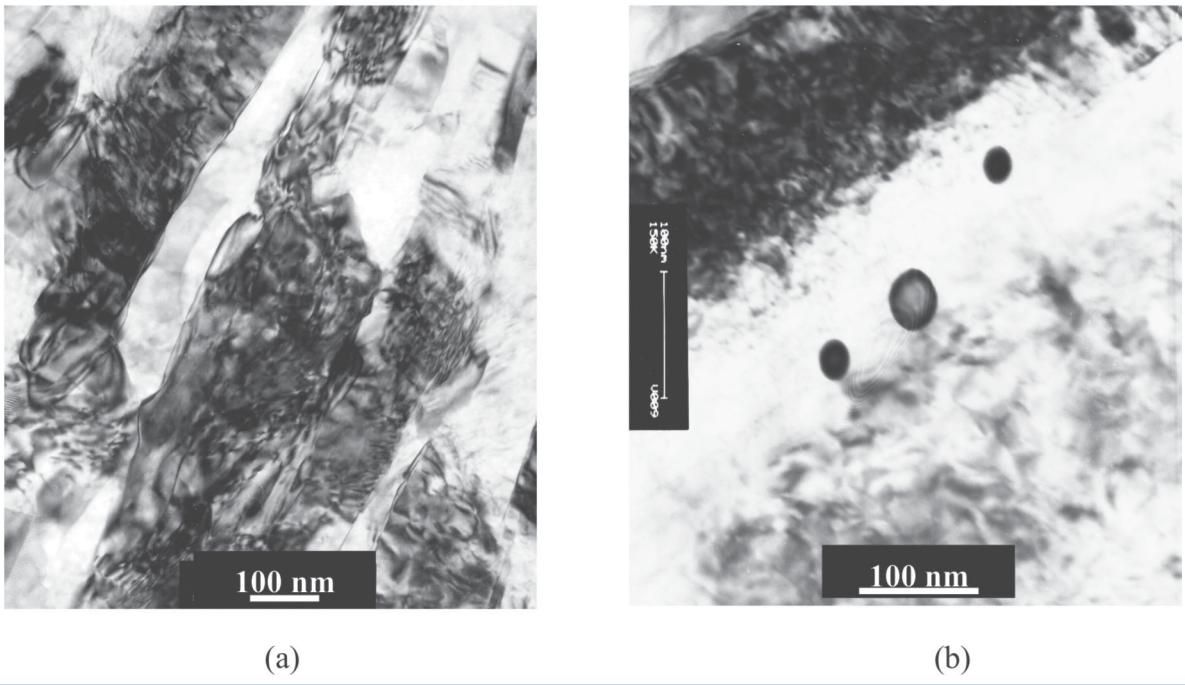

Fig. 7: TEM micrographs of Al-Mg-Si-(Zr) (Alloy 1)and Al-Mg-Si-(Sc-Zr) (Alloy 2), after 12 passes, (a) and (b), respectively.

which tend to form block walls. Thus, either block walls and cell boundaries, formed by increasing severe plastic deformation, flow and slide within the microstructure, primarily by the effect of the specific die geometry [18, 27,28,37-43]. They also adhere to the row of fine dispersoids encountered in their path. This may also explain the markedly smaller fraction of high-angle boundaries (essentially block walls) formed during straining in Alloy 2, compared to Alloy 1. Particles pin the new formed boundaries and, inducing them to follow the previously formed boundaries, contribute to their much pronounced misorientation gradient and, as a consequence, their smaller fraction with respect the material containing a smaller fraction of Al_3Zr dispersoids (Fig. 8).

In a previous manuscript (Cabibbo *et al.* [40]), a breaking-up of Mg_2Si and shrinking of Si particles in a similar 6082-T8 subjected to ECAP was documented. The same investigations were carried out on the Alloy 1 and Alloy 2; results are reported in Table 1, where for a sake of convenience, the data published in [44], and related to the parent Al-Mg-Si T8 alloy, are also reported.

The major aspect is by far the remarkable Mg_2Si size reduction with strain (especially after the first pass), whilst Si particles reduction effect is rather limited. This appear also in the case of Al Alloy 1 than Alloy 2, revealing a Sc-containing dispersoids effect on the microstructural deforming aspects.

The very interesting aspects in the present case are the reduced scale of the former phenomenon following severe plastic deformation, especially in the material containing $Al_3(Sc_{1-x},Zr_x)$ dispersoids, compared to the case presented in [44]. Dispersoids containing particles are believed to be able to inhibit the effect of dislocations in cutting and promoting re-solution of Mg_2Si and Si particles, by effectively pinning them. The $Al_3(Sc_{1-x},Zr_x)$ has by far a predominant role in the material hardening mechanism over all the other particles decorating the microstructure. The rather low volume fraction of both Si and Mg_2Si fine secondary phase particles is basically due to the overaging treatment at 463K/8h, which induces the particle growing to a micrometer scale. These were not taken into account in our analyses due to their far less effectiveness in alloy hardening.

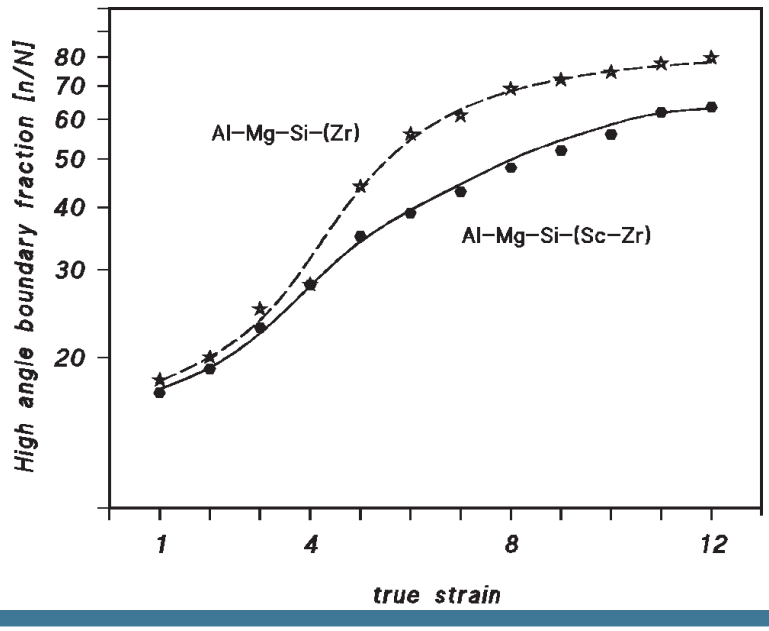

Fig. 8: Comparison of high angle boundary fraction in Alloy 1 and Alloy 2.

Table 2 - Equivalent diameter (d_{EQ}), volume fraction (N_V), subgrain size (l) as a function of strain (number of ECAP passes) for AA6082-Zr (alloy-1), AA6082-Sc-Zr (alloy-2) and commercial AA6082.

Alloy 1		**d_{eq} [nm]****	**N_v [10^{19} / m^3]****	**λ [nm]****
as-extruded + T8	S	130	1.05	1090
	Mg_2Si	*185*	*1.30*	*810*
ECAP 1 pass	Si	118	0.90	1420
	Mg_2Si	*168*	*0.85*	*1160*
ECAP 8 passes	Si	116	0.60	1530
	Mg_2Si	*125*	*0.80*	*1220*
ECAP 12 passes	Si	102	0.45	1810
	Mg_2Si	*115*	*0.50*	*1620*
Alloy 2		**d_{eq} [nm]****	**N_v [10^{19} / m^3]****	**λ [nm]****
aas-extruded + T8	Si	145	1.00	1050
	Mg_2Si	*190*	*1.35*	*780*
ECAP 1 pass	Si	130	0.90	1140
	Mg_2Si	*200*	*0.95*	*900*
ECAP 8 passes	Si	120	0.80	1250
	Mg_2Si	120*165*	*1.20*	*905*
ECAP 12 passes	Si	125	0.95	1160
	Mg_2Si	*160*	*1.05*	*980*
AA6082 ref. [37]		**d_{eq} [nm]****	**N_v [10^{19} / m^3]****	**λ [nm]****
T8	Si	100	1.15	490
	Mg_2Si	*160*	*3.30*	*1390*
ECAP 1 pass	Si	120	0.65	4570
	Mg_2Si	*150*	*0.75*	*3030*
ECAP 4 passes	Si	110	0.65	4540
	Mg_2Si	*135*	*1.15*	*2640*
ECAP 6 passes	Si	100	0.60	4560
	Mg_2Si	*110*	*1.40*	*2660*

Only the nanometre-scale particles are here considered.
**: Associated error: 5%.

CONCLUSIONS

AA1200. Despite the redundant nature of route Bc, up to a total strain of 8, this processing route still gave rise to marked grain refinement. After the maximum strain, the billet contained a bimodal structure of grains fairly larger 1-1.2 mm and submicron grains concentrated in bands. Among the three different processing routes, the material processed via route Bc contained the lowest density of high angle boundaries with a high angle grain boundary fraction of only 30 pct, after a strain of e ≅ 3, and still 25 pct of LABs, after the maximum strain (e ≅ 8).

AA5754. TEM investigation reveals that ECAP is an effective tool for achieving substantial reduction in the grain size. The initial grain size of ≅ 70 μm was reduced to ≅ 0.3–0.4 μm by ECAP after 8 passes at room temperature.

AA6082. Moreover, in the full annealed material the strengthening effect of Si appeared to be predominant over Mg_2Si, whereas in the severely deformed material, the metastable b" particles (precursors of the stable Mg_2Si) revealed a widespread tendency to be fragmented and the finer particles were more effective in pinning the dislocations. By contrast, Si tended to dissolve under SPD and its strengthening effect was drastically reduced.

AA6106 with Zr and Zr+Sc. The major results for these two alloys can be highlighted as follows:

a. The elongated grains of full annealed and overaged, pressed (Sc-Zr)-containing material were thinner respect the ones of the Zr-containing material, the mean transverse grain spacing being ~12mm and ~20 mm, respectively.
b. The presence of the very fine $Al_3(Sc_{1-x},Zr_x)$ dispersoids, in the (Al-Mg-Si)-Zr alloy has highlighted some complex and important effects. The particles effectively reduce the block walls spacing and the cell size, thereby increasing the critical strain required to acquire a sufficiently large fraction of high angle boundaries (essentially block walls) in the microstructure. At the same time, boundary misorientation continuously increased up to a strain of 12, especially for the (Sc-Zr)-containing alloy.
c. An interesting aspect is the reduction of breaking-up of Mg_2Si particles and Si shrinkage, generated by the severe plastic deformation, especially in the material containing $Al_3(Sc_{1-x},Zr_x)$, compared with the parent AA6082.

ACKNOWLEDGMENTS

The author wish to acknowledge Prof. H. McQueen and Prof. Ryum for fruitful discussion.

REFERENCES

1. V.M. Segal, Mater.Sci. Eng. A, 1995, 197, 157.
2. Y.T. Zhu, T.C. Lowe, Mater. Sci. Eng., A,, 2000, 291, 46.
3. V.M. Segal, V.I. Reznikov, A.E. Drobyshevskiy, V.I. Kopylov, Russian Metallurgy, 1981, 1, 99.
4. S.C. Baik, Y. Estrin, H.S. Kim, R.J. Hellmig, Mater. Sci. Eng. A, 2003, 351, 86.
5. P.B. Berbon, N.K. Tsenev, R.Z. Valiev, M. Furukawa, Z. Horita, M. Nemoto, T.G. Langdon, Metall. Mater. Trans. A, 1998, 29, 2237.
6. Y. Iwahashi, Z. Horita, M. Nemoto, T.G. Langdon, Acta Mater., 1998, 46, 3317.
7. P.B. Prangnell, J.R. Bowen. Ultrafine Grained Materials-II, Ed. Y.T. Zhu, T.G. Langdon, R.S. Mishra, S.L. Semiatin, M.J. Saran, T.C. Lowe, TMS (The Minerals, Metals & Materials Society) , 2002, 89.
8. A. Gholina, P.B. Prangnell, M.V. Markushev, Acta Mater., 2000, 48, 1115.
9. J.Y. Chang, J.S. Yoon, G.H. Kim, Scripta Mater., 2001, 45, 347.
10. Z. Horita, T. Fucinami, M. Nemoto, T.G. Langdon, Metall. Mater. Trans. A, 2000, 31, 691.
11. Y. Iwahashi, M. Furakawa, Z. Horita, M. Nemoto, T.G. Langdon, Metall. Mater. Trans. A, 1998, 29, 2245.
12. M. Furukawa, Z. Horita, M. Nemoto, R.Z. Valiev, T.G. Langdon, Acta Mater., 1996, 44, 4619.
13. M. Furukawa, Z. Horita, T.G. Langdon, Mater. Sci. Eng. A, 2002, 332, 97.
14. P.L. Sun, P.W. Kao, C.P. Chang, Scripta Mater., 2004, 51, 565.
15. P.L. Sun, P.W. Kao, C.P. Chang, Metall. Mater. Trans. A, 2004, 35, 1359.
16. Y.T. Zhu, T.C. Lowe, Mater. Sci. Eng. A, 2000, 291, 46.
17. J.A. Wert, Q. Liu, N. Hansen, Acta Mater., 1997, 45, 2565.
18. D.A. Hughes, Mater. Sci. Eng. A, 2001, 319-321, 46.
19. Q. Liu, X. Huang, D.J. Lloyd, N. Hansen, Acta Mater., 2002, 50, 3789.
20. P.J. Hurley, P.S. Bate, F.J. Humphreys, Acta Mater., 2003, 51, 4737.
21. H. Weiland, Acta Metall., 1992, 40, 1083.
22. A. Godfrey, D.A. Hughes, Acta Mater., 2000, 48, 1897.
23. Q. Liu, N. Hansen, Scripta Metall. Mater., 1995, 32, 1289.
24. D. Kuhlmann-Wilsdorf, N. Hansen, Scripta Metall., 1991, 25, 1557.
25. N. Hansen, D. Juul Jensen, Acta Metall., 1992, 40, 3265.
26. D. Kuhlmann-Wilsdorf, Mater. Sci. Eng. A, 1989, 113, 1.
27. D.A. Hughes, N. Hansen, Acta Mater., 2000, 48, 2985.
28. D.A. Hughes, N. Hansen, Acta Mater., 1997, 45, 3871.
29. B. Bay, N. Hansen, D.A. Hughes, D. Kuhlmann-Wilsdorf, Acta Metall. Mater., 1992, 40, 205.
30. M.F. Ashby, Phil. Mag., 1970, 21, 399.
31. D.A. Hughes, M.E. Kassner, M.G. Stout, J. Vetrano, J. Metals, 1998, 50, 16.
32. R.D. Doherty, D.A. Hughes, F.J. Humphreys, J.J. Jonas, D. Juul Jensen, M.E. Kassner, W.E. King, T.R. McNelley, H.J. McQueen, A.D. Rollett, Mater. Sci. Eng. A, 1997, 238, 274.
33. D.N. Seidman, E.A. Marquis, D.C. Dunand, Acta Mater., 2002, 50, 4021.
34. V.G. Davydov, T.D. Rostova, V.V. Zakharov, Y.A. Filatov, V.I. Yelagin, Mater. Sci. Eng. A, 2000, 280, 30.
35. A. Tolley, V. Radmilovic, U. Dahmen, Scripta Mater., 2005, 52, 621.
36. Q. Liu, H. Xiaooxu, Y. Mei, Ultramicroscopy, 1992, 41, 317.
37. M. Cabibbo, E. Evangelista, V. Latini, J. Mater. Sci., 2004, 39, 5659.
38. M. Cabibbo, E. Evangelista and C. Scalabroni: Micron, 2005, 36, 5, 401.
39. Langdon
40. M. Cabibbo, E. Evangelista and M. Vedani: Metall. Mater. Trans. A, 2005, 36, 5, 1353.
41. M. Cabibbo and E. Evangelista: Proc. of ICAA-9, ed. IMEA, Brisbane, Australia, 2004, 190.
42. M. Vedani, P. Bassani, M. Cabibbo, V. Latini, E. Evangelista: Metall. Sci. Techn., 2003, 21, 3.
43. M. Cabibbo, E. Evangelista: J. Mater. Sci., in press.
44. J. Wang, Y. Iwahashi, Z. Horita, M. Furukawa, M. Nemoto, R.Z. Valiev, T.G. Langdon, Acta Mater., 1996, 44, 2973.